01 Jun 1999

Oxygen and Phosphorus Coordination Around Iron in Crystalline Ferric Ferrous Pyrophosphate and Iron-phosphate Glasses with UO_2 or Na_2O

C. H. Booth

P. G. Allen

J. J. Bucher

N. M. Edelstein

et. al. For a complete list of authors, see https://scholarsmine.mst.edu/matsci_eng_facwork/1449

Recommended Citation

C. H. Booth et al., "Oxygen and Phosphorus Coordination Around Iron in Crystalline Ferric Ferrous Pyrophosphate and Iron-phosphate Glasses with UO_2 or Na_2O," *Journal of Materials Research*, Materials Research Society, Jun 1999.
The definitive version is available at https://doi.org/10.1557/JMR.1999.0352

Journal of
MATERIALS RESEARCH

Oxygen and phosphorus coordination around iron in crystalline ferric ferrous pyrophosphate and iron-phosphate glasses with UO_2 or Na_2O

C. H. Booth,[a] P. G. Allen,[b] J. J. Bucher, N. M. Edelstein, and D. K. Shuh
Chemical Sciences Division, Lawrence Berkeley National Laboratory, Berkeley, California 94720

G. K. Marasinghe, M. Karabulut, C. S. Ray, and D. E. Day
Department of Physics, Department of Ceramic Engineering, and the Graduate Center for Materials Research, University of Missouri, Rolla, Missouri 65409

(Received 19 August 1998; accepted 17 February 1999)

Fe *K*-edge x-ray absorption fine-structure (XAFS) measurements were performed on glass samples of $(Fe_3O_4)_{0.3}(P_2O_5)_{0.7}$ with various amounts of Na_2O or UO_2. Near-edge and extended XAFS regions are studied and comparisons are made to several reference compounds. We find that iron in the base glass is ~25% divalent and that the Fe^{2+} coordination is predominantly octahedral, while Fe^{3+} sites are roughly split between tetrahedral and octahedral coordinations. Also, we measure roughly one Fe–O–P link per iron. Substitution of Na_2O or UO_2 up to 15 mol% primarily affects the first Fe–O shell. The results are compared to data from the related material $Fe_3(P_2O_7)_2$.

I. INTRODUCTION

Iron-phosphate glasses have many advantages over other phosphate glasses as a high-level nuclear waste storage medium.[1–4] One important advantage is the excellent chemical durability, which is comparable to or better than that of borosilicate glasses. For lead-iron-phosphate glasses, this durability is manifest by leach rates in aqueous solutions with pH between ~5 and 9 that are 100–1000 times lower than in borosilicate glasses,[1,3] which encompasses almost all natural ground waters. Iron-phosphate glasses maintain this durability even when moderate amounts (~15 wt%) of simulated nuclear waste (including nonradioactive constituents) are vitrified into the glass.[3,4] This durability has made iron-phosphate glasses an alternative to methods currently under consideration by the United States Department of Energy for storage of high-level nuclear waste that contains significant amounts of iron and phosphorus.[5] Other important advantages over the borosilicate glasses include a low melting point (~800 °C), no tendency to devitrify at repository temperatures, and the abundance of Fe_2O_3 and P_2O_5 in nuclear waste streams.[1] The latter point means that less additional material is needed to vitrify some waste, and therefore the overall volume of the waste form is smaller.

Several models have been proposed to explain why a phosphate glass (normally easily hydrated) should become resistant to hydration when iron in added. Phosphate glasses typically include a backbone of $(PO_4)^{3-}$ chains. It is generally recognized that minimizing the number of P–O–P links between $(PO_4)^{3-}$ tetrahedra (that is, linked via bridging oxygens, or BOs), while maximizing the more robust Fe–O–P links (nonbridging oxygens, or NBOs) is important.[2] The additional iron may act to strengthen cross-links between chains and may also shorten chain length. Another important benefit of adding iron is the overall densification of the glass. Most phosphate glasses tend to form rings of PO_4^{3-} tetrahedra which create large, open channels through which small ions (such as H_3O^+ ~ 1 Å) can diffuse. The introduction of iron may cause "knots" to form that constrict these channels.[6] Clearly, a central factor in characterizing phosphate waste glasses is determining the relative number of BOs to NBOs in a given glass.

The proposed models underscore the importance of understanding the local structure of the iron-phosphate glasses for determining the mechanisms of chemical durability and other properties. Infrared (ir) spectroscopy has been employed as a vibrational probe of the various P–O–P and Fe–O–P combinations in $Fe_2O_3 \cdot 1.25P_2O_5$.[7] Infrared measurements on $Fe_2O_3 \cdot P_2O_5 \cdot Na_2O$ glasses have shown that the amplitude of the P–O–P spectral features decreases with increasing Fe content,[8] possibly indicating that the length of such PO_4^{3-} chains is reduced in their glasses. Liquid chromatography has identified chains containing up to 13 units of PO_4^{3-} tetrahedra in lead-iron-phosphate solutions, and has shown that the average chain length decreases with increasing iron concentration.[4] Raman measurements have observed an asymmetric broadening of the dominant band at $\Delta\nu = 1150\ cm^{-1}$ that increases with iron concentration,[4] probably indicating the creation of $O=P_3^{2-}$ end groups and $O=P_3^{3-}$ orthophosphate groups.

[a]Address all correspondence to this author. Present address: Los Alamos National Laboratory, MS K764, Los Alamos, New Mexico 87545. e-mail: cbooth@lanl.gov
[b]Present address: Lawrence Livermore National Laboratory, P.O. Box 808, MS L-231, Livermore, California 94551.

A useful model compound for exploring these hypotheses is ferric ferrous pyrophosphate [$Fe_3(P_2O_7)_2$, Fig. 1], which has a single P–O–P link between two PO_4 tetrahedra.[9] The pyrophosphate $(P_2O_7)^{4-}$ structures are linked via FeO_{12} clusters which consist of two Fe^{3+} distorted octahedra, each sharing a face with one Fe^{2+} trigonal prism. Even though there is a remaining P–O–P link between the two tetrahedra in P_2O_7, the same tetrahedra are also linked via P–O–Fe–O–P paths, just as the P_2O_7 groups are linked to each other. There are no channels as large as an H_3O^+ ion (~1 Å) in this lattice. These structural features make $Fe_3(P_2O_7)_2$ an excellent model of the ideal next-nearest-neighbor local structure for the iron-phosphate waste glass. In addition, pyrophosphate is known to crystallize from melts of the same composition as the glasses by annealing at different temperatures.

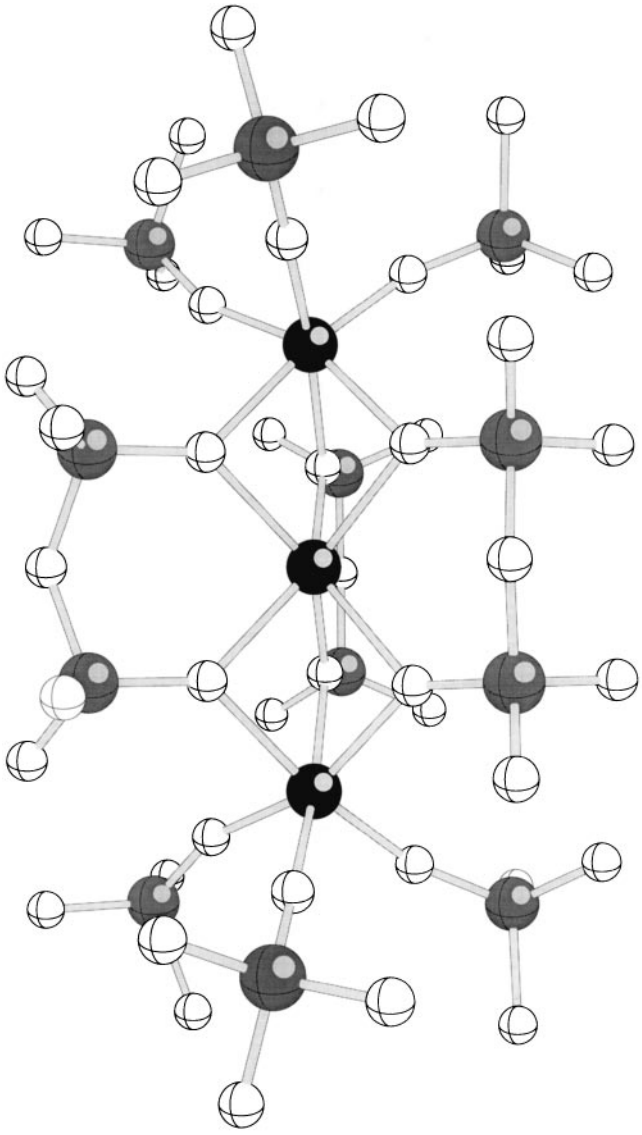

FIG. 1. Crystal structure of $Fe_3(P_2O_7)_2$ (ferric ferrous pyrophosphate) as reported in Ref. 9. The black atoms are iron, gray are phosphorus, and white are oxygen. The central iron is Fe^{2+} and sits in a trigonal prism of oxygens. The remaining irons are Fe^{3+} and sit in a distorted octahedron of oxygens.

Although $Fe_3(P_2O_7)_2$ may be a useful model crystal for characterizing Fe–O–P linkages, the nearest-neighbor oxygen coordination may be different in the glasses and still preserve the linkages. Mössbauer spectroscopy is an excellent probe for examining local structure around iron. Mössbauer studies have been performed on lead-phosphate and sodium-containing iron-phosphate glasses,[8,10] as well as on $Fe_3(P_2O_7)_2$ polycrystals,[11] with interesting results. The spectra from these related materials are best modeled as a combination of Fe^{2+} and Fe^{3+} sites. The predominant coordination of oxygen around iron in the glasses is octahedral, although at least one study identifies a probable tetrahedral Fe^{3+} site for $(Fe_2O_3)_x(P_2O_5)_y(Na_2O)_z$ that changes with iron and sodium concentration.[8] Other Mössbauer research finds that $(1 - x)NaPO_3 \cdot xFe_2O_3$ glasses are best characterized by two distinct octahedral Fe^{3+} sites.[10] In a recent study comparing neutron and x-ray powder diffraction results with Mössbauer results from an $(Fe_2O_3)_{0.4}(P_2O_5)_{0.6}$ glass and $Fe_3(P_2O_7)_2$ made from the same starting composition, spectral features attributed to the trigonal prism in $Fe_3(P_2O_7)_2$ were not present in the glass.[11]

Although general site symmetries and coordination geometries can sometimes be roughly inferred from the above experiments, a local-structure probe is necessary to determine the local atomic environment around iron. Radial-distribution function analysis of x-ray diffraction data has demonstrated 6-fold oxygen coordination around iron in lead-iron-phosphate glasses with 6–9 wt% Fe content.[12] Extended x-ray absorption fine-structure (EXAFS) measurements have also been previously performed on lead-iron-phosphate glasses.[6] Even so, given that previous Mössbauer, diffraction, and EXAFS experiments have often been unable to unambiguously assign certain spectral features to particular local environments in these systems, it will be very useful to find a systematic way of determining coordination geometries.

The primary focus of this study is to provide details about the iron site valences, coordinations, and Fe–P environment (implying Fe–O–P links) in iron-phosphate glasses and to correlate the structural properties with the physical and chemical properties of the respective glasses. To this end, we have employed the x-ray absorption fine-structure (XAFS) technique on a variety of iron-phosphate samples. These glasses form a series starting with a base glass of composition $31Fe_3O_4 \cdot 69P_2O_5$ and including up to 15 mol% of either Na_2O or UO_2. We also collected data on a polycrystalline sample of $Fe_3(P_2O_7)_2$ which was crystallized from the same starting composition as the base glass. All of

these samples have been previously characterized by thermogravimetric, x-ray diffraction, x-ray photoelectron spectroscopy, and Mössbauer analyses.[11] We have analyzed the Fe *K*-edge absorption spectrum in the near-edge region (x-ray absorption near-edge structure, or XANES) and in the post-edge region (EXAFS). In addition, we have collected data on a wide variety of iron-oxide reference compounds. These data allow the determination of oxidation states, the local structure around a given atomic species, and the origins of some electronic features.

We describe the experimental details in Sec. II, report the results in Sec. III, discuss the results of the measurements, how they relate to each other and how they compare to other measurements in Sec. IV, and give the main conclusions in Sec. V.

II. EXPERIMENTAL DETAILS

A. Sample preparation and experimental details

The glasses were synthesized by melting homogeneous mixtures of reagent grade chemicals in dense alumina crucibles in air at 1200 °C for approximately 2 h. A base glass was prepared from 31% Fe_3O_4 and 69% P_2O_5 (all percentages are mol% unless specified otherwise). A series of glasses was made by melting ~5, 10, or 15% of UO_2 with the base glass composition. A second series was made by melting similar amounts of Na_2O with the base glass. Each melt was quenched in air by pouring into steel molds. Rectangular samples were immediately transferred to an annealing furnace and annealed at 450 °C for 3 h. Polycrystalline $Fe_3(P_2O_7)_2$ and (partly) $Fe_4(P_2O_7)_3$ were obtained by heating parts of the base glass for approximately 24 h at 650 or 800 °C, respectively. Diffraction patterns indicate that the glass samples have no long-range order. Rietveld analysis on the nominally $Fe_3(P_2O_7)_2$ polycrystal indicates the presence of 5–10% amorphous phase, with the remaining structural component in good agreement with the previously published structure of $Fe_3(P_2O_7)_2$.[9] The partly $Fe_4(P_2O_7)_3$ sample was found to be ~77% $FePO_4$ and ~23% $Fe_4(P_2O_7)_3$.[13] Due to the mixed-phase nature of this sample, we refer to this sample as $M40x$. The refined structure for $Fe_4(P_2O_7)_3$ will be presented in a future paper.

Appropriate reference materials include FeO, Fe^{2+} in 1.5 M $HClO_4$, $FePO_4 \cdot xH_2O$,[14] Fe_2O_3, and Fe_3O_4. These materials have iron in a variety of valence states and oxygen coordinations. However, none of these materials has a single-site, tetrahedrally coordinated iron. To obtain a sample with tetrahedral coordination, we heated part of the $FePO_4 \cdot xH_2O$ powder in an open quartz tube at 600 °C for 6 h.[15] An x-ray diffraction pattern indicates the resulting sample is single phase (>98%) $FePO_4$, which has a tetrahedral coordination of oxygen around Fe^{3+} sites.

X-ray absorption spectra were collected at room temperature on beam line 4-1 at the Stanford Synchrotron Radiation Laboratory (SSRL) at the Fe *K*-edge in transmission mode using Si(220) monochromator crystals. The powder samples were mixed with polystyrene beads and loaded into an aluminum holder with kapton windows such that the samples were ~0.7 absorption lengths thick. Data were reduced and fit using standard procedures.[16,17] An iron foil was used as an internal energy reference. The first inflection point of the absorption of the foil was defined to be at 7112 eV.

B. Fitting procedures

The iron oxidation state is determined by measuring the Fe *K*-edge excitation energy (E_0) of the glasses and interpolating these energies between those of the reference compounds. The threshold energy E_0 shifts linearly with valence because of the change in the number of available screening electrons (see Ref. 18 for a more thorough treatment). Because the local electronic environment also affects E_0, the proper choice of reference materials is important. With a proper choice, interpolating the edge energies usually gives the effective valence to ~0.03 valence units. We measure E_0 in this study by estimating the size of the step in the absorption edge and measuring the energy at the half-height of the absorption. The edge step magnitude is determined by linearly extrapolating the region from 7200–7400 eV to intersect the main edge. This method of determining E_0 avoids complications due to changes in the magnitude of pre-edge features (for instance, from varying separate Fe^{2+} and Fe^{3+} contributions that occur in the glasses we wish to study) which affect the interpretation of choosing E_0 from, say, the first inflection point in the edge. For example, if one wants a measure of the iron valence in Fe_3O_4, good Fe^{2+} and Fe^{3+} references are the edge energies from FeO and Fe_2O_3, respectively. We measured a shift in E_0 of the Fe *K*-edge (taken at the half-height of the edge) between FeO and Fe_2O_3 of 3.77 eV. The edge energy of iron in Fe_3O_4 is 2.57 eV greater than FeO, giving an effective valence (nominally +2.67) of $2 + 2.57/3.77 = +2.68$ (3).

Features in the pre-edge region of the Fe *K*-edge near 7115 eV are sensitive to both coordination and site symmetry. This resonance is primarily due to a $1s \rightarrow 3d$ transition, which is dipole allowed by hybridization of *p* and *d* states, and also by quadrupole transitions. Studies of transition-metal compounds have shown that such excitations are generally present[18–20] if empty *d* states are available,[22] and are minimized by ideal octahedral coordination (which forbids *p*-*d* mixing). Recent ligand field calculations have shown that these features are

described well by crystal field theory,[20] and in particular, that in an octahedral field, the feature displays two lobes split by an energy corresponding to the octahedral-field splitting. Calculations utilizing a more thorough multiple-scattering formalism (taking into account larger atom clusters) are also being performed.[21] Unfortunately, interpreting the XANES within these theories requires a more thorough experimental and theoretical understanding of the pre-edge features, which has not yet been established. Comparisons to model systems still produce the most reliable interpretations.

To quantify the pre-edge features, fits to the edge were performed with an integrated Lorentzian for the main edge ($m.e.$) (no Gaussian character was necessary) and pseudo-Voigt peaks ($p.V.$) for the other excitations:

$$\mu_{p.V.} = A\left[me^{(E-E_m)^2/2W^2} + (1-m)\frac{W^2}{W^2+(E-E_m)^2} \right],$$

where E_m is the energy of the $1s \rightarrow 3d$ excitation, A is the overall amplitude of the excitation, W is the width of both the Gaussian and the Lorentzian contributions (taken to be equal for simplicity), and m is the ratio of those parts. The resolvable excitations should be Lorentzian in character. However, it is important to recognize the core-hole lifetime broadening with respect to the monochromator resolution. The Fe K-edge core width is 1.33 eV,[23] and the monochromator resolution is ~0.5 eV, so single-transition excitations should be predominantly Lorentzian.

EXAFS analyses focus on the oscillatory fine structure above the absorption edge. This structure is isolated by fitting a smooth function through $\mu(E)$ to give $\mu_0(E)$ above the edge and calculating $\chi(E) = \mu(E)/\mu_0(E) - 1$. Structure in χ results from the interference of the outgoing part of the photoelectron wave function and the part backscattered off neighboring atoms. The oscillation frequency of χ (with the photoelectron wave vector k given by $E - E_0 = \hbar^2k^2/2m_e$) is proportional to the distance from the absorber to the backscattering atom, and the amplitude is proportional to the number of neighbors. Fits to χ therefore give information about the number of neighbors, the distance, and the distribution width of a shell of atoms around the absorbing atomic species. Identification of the species of backscattering atom is also possible by observing the shape of the scattering amplitude and phase shifts with k.

Data were fit to the Fourier transform (FT) of $k^n\chi(k)$ between 1 and 3.3 Å. Reported results are averages of fits to various models with $n = 1$ and $n = 3$. Backscattering amplitudes and phases were calculated using the FEFF6[24] multiple scattering code on an $Fe_3(P_2O_7)_2$ cluster[9] for all single scattering paths up to Fe–P (~3.4 Å). An overall amplitude reduction factor $S_0^2 = 0.75(5)$ was determined from the reference materials and used throughout the subsequent analysis.

III. RESULTS

A. XANES measurements

1. Main edge

For the best comparison to the iron-phosphate glasses, crystalline iron-phosphate reference materials that have only Fe^{2+} or Fe^{3+} in them should be used. Thus, the ideal compounds would be ferrous pyrophosphate $Fe_2P_2O_7$ and ferric pyrophosphate $Fe_4(P_2O_7)_3$, respectively. Single-phase samples of these pyrophosphates could not be obtained, so FeO was used as the Fe^{2+} standard and the $M40x$ sample was used as the Fe^{3+} standard. E_0 for iron in $M40x$ is 4.21 eV higher than iron in FeO. E_0 for $M40x$ is 0.39 eV higher than in $FePO_4$.

Figure 2 shows the absorption edges from the references (FeO, $M40x$), $Fe_3(P_2O_7)_2$, and the base glass. Interpolation between E_0 for these materials indicates the iron valence is +2.75(3) for the base glass and +2.82(3) for the $Fe_3(P_2O_7)_2$ polycrystal. These measurements are in quantitative agreement with Mössbauer measurement,[11,25] subject to E_0 for FeO and $M40x$ being similar (~0.2 eV) to E_0 in $Fe_2P_2O_7$ and $Fe_4(P_2O_7)_3$, respectively. The iron valence in pure $Fe_3(P_2O_7)_2$ is nominally +2.67. The extra 15% of Fe^{3+} is presumably from contributions by the small amount of amorphous phase detected by diffraction.[11]

The same procedures were applied to the base glass series with added UO_2 or Na_2O. The threshold energy changes across the series from 7123.58 to 7122.84 eV.

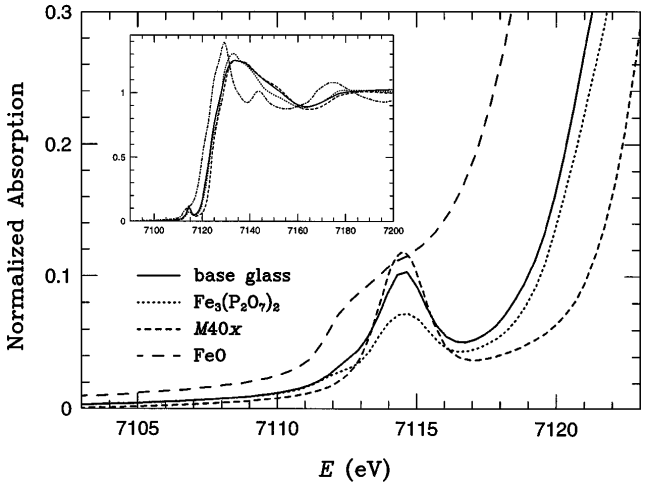

FIG. 2. Absorption (normalized to the step height) versus E (incident photon energy) for the base glass, $Fe_3(P_2O_7)_2$, $M40x$ (Fe^{3+} reference), and FeO (Fe^{2+} reference). The measured absorption μt for each spectra is normalized to unity at the edge step. The main plot highlights the pre-edge region, where the feature at ~7115 eV results from a $1s \rightarrow 3d$ transition. The inset shows the full edge step.

The 15% UO_2 glass therefore has the highest effective iron valence and the 15% Na_2O glass has the lowest of all the measured glasses. Figure 3 shows the oxidation state of iron determined from the edge shifts. These data are in excellent agreement with Mössbauer measurements.[11] $M40x$ appears to be a good Fe^{3+} reference material for the glass and the ferric ferrous pyrophosphate samples, since all these valence measurements agree well with Mössbauer results.

2. Pre-edge

Reference materials. To interpret the pre-edge features in the iron-phosphate data, we have measured several reference iron oxides possessing various oxygen coordinations. In the noncrystalline reference samples Fe^{2+} in 1.5 M $HClO_4$ and $FePO_4 \cdot xH_2O$, the EXAFS show that the oxygen environment is well ordered ($\sigma_{DW} \sim 0.05$ Å), the number of neighbors is 6.0 ± 0.3, and the bond-valence sum[26] and main edge independently determine valences of $+2$ and $+3$, respectively. We therefore assume that the oxygen coordination in these materials is undistorted octahedral. The oxygen coordinations of iron in the crystalline compounds are undistorted octahedral around Fe^{2+} in FeO, distorted octahedral around Fe^{3+} in Fe_2O_3 (three oxygens at 1.9 Å and three at 2.1 Å), and undistorted octahedral around two Fe^{3+} sites together with an undistorted tetrahedron around one Fe^{2+} site in Fe_3O_4. In addition, iron in $FePO_4$ is trivalent and in an undistorted tetrahedral coordination; EXAFS analysis confirms the coordination. We therefore have three references with a well-ordered nearest-neighbor oxygen shell. The other references will be used to consider the effects of their distortions. Figure 4 shows the pre-edge feature from some of the reference compounds with the main edge removed. The FeO data were collected with poorer resolution than the Fe^{2+} in 1.5 M $HClO_4$ data, so only the latter is shown (see Fig. 2 and Table I for FeO results). Data from $FePO_4$ are shown in Fig. 5(a). Since each sample in Fig. 4 has at least some octahedral character, the double-lobed signature of the crystal field splitting into e_g and t_{2g} levels is noticeable in all of the spectra. The largest feature occurs for tetrahedral $FePO_4$, but one should note how large the peaks can be for distorted octahedrons, as in Fe_2O_3.

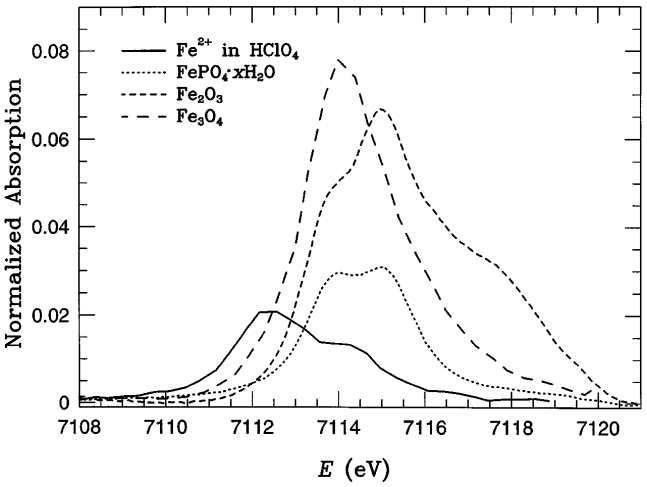

FIG. 4. Normalized absorption versus E with main edge removed for the reference compounds Fe^{2+} in 1.5 M $HClO_4$ (solid, Fe^{2+} octahedral), $FePO_4 \cdot xH_2O$ (dotted, Fe^{3+} octahedral), Fe_2O_3 (short dashed, Fe^{3+} distorted octahedral), and Fe_3O_4 (long dashed, Fe^{2+} and Fe^{3+} sites, see text).

Table I gives results of the fits to the pre-edge feature of all the reference compounds. The data from each of the octahedral-coordinated reference compounds require at least two pseudo-Voigt peaks to obtain a good fit, with the Fe_2O_3 data requiring three peaks. The data from tetrahedral-coordinated $FePO_4$ requires only a single, large peak to obtain a good fit. The extra peak in Fe_2O_3 (centered at 7117.2 eV) may be indicative of the off-center displacement of the iron toward a face center of the octahedron. The main peak in the Fe_3O_4 data coincides with the left lobe in the $FePO_4 \cdot xH_2O$ data. Since two of the three irons in Fe_3O_4 reside in a similar environment as in $FePO_4 \cdot xH_2O$, $2/3 \times A_{1st\ peak} \sim 25\%$ of the main peak area in the Fe_3O_4 data should arise from the octahedral sites. The rest of this amplitude should be the contribution from the tetrahedral site. This signal corresponds to an amplitude of 0.14(2) per tetrahedral iron, which agrees reasonably well with the amplitude of the tetrahedral signal from $FePO_4$ of 0.18(1). As previously mentioned, the undistorted octahedra have the smallest features, although the feature is stronger in the Fe^{3+} data from $FePO_4 \cdot xH_2O$ than in the Fe^{2+} data from Fe^{2+} in 1.5 M $HClO_4$. This difference is probably because the Fe^{3+} has more available empty d states than

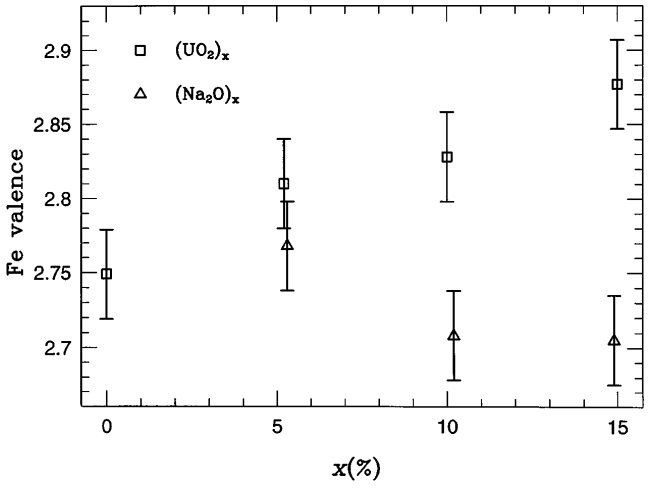

FIG. 3. Mean iron valence versus UO_2 or Na_2O concentration x, as measured by the edge position for the glass series.

TABLE I. Fit results of pseudo-Voigt peaks to the pre-edge feature in reference compounds. A is the overall amplitude, E_m is the mean energy of the peak, W is the half-width (taken to be the same in both the Lorentzian and the Gaussian parts), and m is the ratio of the relative amplitudes of the Gaussian and the Lorentzian parts. Errors for the last digit(s) are reported in parentheses, and are determined from the covariance matrix and by assuming they are normally distributed.

	1st peak				2nd peak				3rd peak			
Sample	A	E_m	W	m	A	E_m	W	m	A	E_m	W	m
FeO	0.03 (1)	7113.1 (7)	0.97(8)	1 (1)	0.017(8)	7115 (1)	1.0 (1)	1 (1)				
$Fe^{2+} \cdot xHClO_4$	0.020(1)	7112.42(4)	0.94(4)	0.4(2)	0.010(3)	7114.35(7)	0.9 (5)	0.05(1)				
Fe_3O_4	0.064(10)	7114.0 (4)	0.83(4)	0.6(3)	0.029(5)	7115.4 (5)	1.3 (2)	0.2 (9)				
Fe_2O_3	0.030(6)	7113.7 (3)	0.75(9)	1.0(3)	0.052(7)	7115.0 (2)	0.9 (5)	0.3 (9)	0.028(7)	7117.2(3)	1.3(2)	1.0(2)
$FePO_4 \cdot xH_2O$	0.021(1)	7113.83(4)	0.72(6)	0.0(2)	0.026(1)	7115.10(4)	0.87(6)	0.0 (2)				
$FePO_4$	0.18 (1)	7114.45(3)	0.82(5)	0.3(1)								

Fe^{2+}. In Fe_2O_3, the features have similar character but are much larger.

Base glass and ferric ferrous pyrophosphate. Figure 5 shows the pre-edge feature for the pyrophosphate polycrystal and the base glass, together with the fitted curves, and Table II shows the fit results. Comparing these data, we find that while both the glass and the $Fe_3(P_2O_7)_2$ data have a small lobe at 7112.4 eV below the main lobe at 7114.5 eV, the relative size of the two features is different. The pre-edge feature is a different shape in these materials than in any of the reference compounds, probably due to inequivalent iron sites, in accord with the mixed-valence state of the iron.

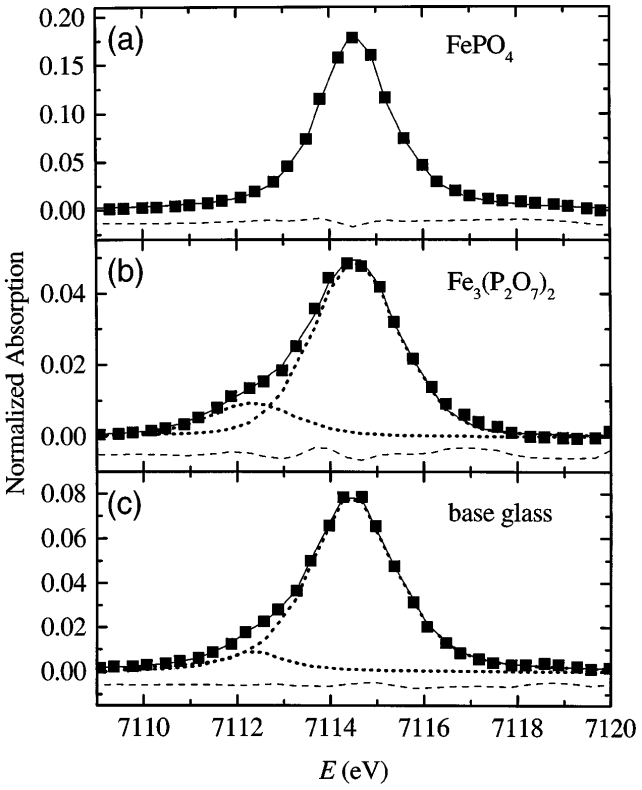

FIG. 5. Normalized absorption versus E with main edge removed for (a) the $FePO_4$ polycrystal, together with a 1-peak fit, (b) the $Fe_3(P_2O_7)_2$ polycrystal, together with a 2-peak fit, and (c) the base glass with a 2-peak fit. Each plot shows data (solid), individual fitted peaks (dotted), total fit (squares), and the fit residue (dashed). The residue is offset for clarity. Notice the different y-axis scales.

Mössbauer data[11] have shown that the Fe^{2+} site goes from a trigonal prism in the crystal to some other coordination in the glass. These XANES pre-edge fit results indicate that the oxygen coordination around the irons in the glass is more distorted from an ideal octahedron relative to the Fe^{3+} sites in $Fe_3(P_2O_7)_2$, possibly even to a tetrahedron. In fact, the position of the feature in tetrahedral $FePO_4$ is very similar to the higher-energy peak in the glass. One can model the pre-edge features of the glass by assuming that the main peak in the glass is dominated by tetrahedral-coordinated Fe^{3+} sites and the lower-energy peak is only from octahedral coordination around Fe^{2+} sites. Within this model, we estimate that roughly $1/3$ of the iron is $+3$ and in a tetrahedral coordination. Although the energy positions and relative amplitudes agree with this model, one could alternatively assume that the main peak in the glass arises from a distortion of the octrahedral sites that differs from any of the reference materials. EXAFS data will be presented below to clarify this situation.

Effect of adding UO_2 and Na_2O. Figure 6 shows the pre-edge feature as a function of UO_2 and Na_2O concentration in the base glass, and Table II shows the fit results. The amplitude of the main (second peak) feature increases with increasing UO_2 and decreases with increasing Na_2O. The position of the main peak at 7114.5 eV changes slightly with x, although this could be an artifact from fitting the main edge. The position of the smaller peak does not change as a function of concentration within the experimental error. The main changes occur in the amplitudes of the peaks and in the amount of Gaussian/Lorentzian character m. The amplitude of the first peak is somewhat insensitive to addition of Na_2O to the glass, increasing by 10–20% at 15% Na_2O. On the other hand, adding 5% or more UO_2 reduces this amplitude such that it is essentially zero. The most evident difference in the pre-edge feature is the

TABLE II. Fit results of pseudo-Voigt peaks to the pre-edge feature in the iron-phosphate glasses and pyrophosphate polycrystals.

	1st peak				2nd peak			
Sample	A	E_m	W	m	A	E_m	W	m
$Fe_3(P_2O_7)_2$	0.009(2)	7112.3 (2)	1.00(4)	0.5 (5)	0.049(2)	7114.56(4)	0.960(4)	0.7 (2)
Base glass	0.010(2)	7112.4 (1)	0.77(24)	0.04(5)	0.079(1)	7114.48(2)	0.965(1)	0.45(9)
5.2% UO_2	0.004(3)	7112.4 (3)	0.55(1)	0.5 (5)	0.097(3)	7114.50(2)	0.974(13)	0.19(10)
10.0% UO_2	0.004(2)	7112.4 (2)	0.5 (5)	0.5 (5)	0.101(2)	7114.51(2)	0.972(1)	0.21(10)
15.0% UO_2	0.002(4)	7112.4 (4)	0.25(1)	0.5 (5)	0.109(4)	7114.57(2)	0.985(42)	0.1 (1)
5.3% Na_2O	0.010(1)	7112.37(7)	0.82(11)	0.0 (5)	0.069(1)	7114.48(1)	0.955(1)	0.61(7)
10.2% Na_2O	0.012(1)	7112.39(6)	0.81(7)	0.1 (4)	0.058(1)	7114.47(1)	0.957(1)	0.78(10)
14.9% Na_2O	0.012(1)	7112.34(7)	0.84(2)	0.2 (4)	0.052(1)	7114.43(2)	0.965(1)	0.88(12)

change in amplitude of the second peak. Adding Na_2O decreases this amplitude by ~45%, while adding UO_2 increases the amplitude by ~72%. Another interesting result is that the character of the peak becomes more Gaussian as Na_2O is added, while adding UO_2 makes the peak more Lorentzian. The amplitude of the main peak in the data from the 10.2% Na_2O sample strongly resembles the main peak from the $Fe_3(P_2O_7)_2$ data (Fig. 5), although the lower-energy shoulder is smaller by more than a factor of 2.

B. EXAFS measurements

1. Ferric ferrous pyrophosphate

To understand the local structure of the iron-phosphate glasses, we have performed a detailed EXAFS analysis of the $Fe_3(P_2O_7)_2$ polycrystal. Since the crystal structure of this material is known,[9] we are able to compare diffraction measurements on this rather complicated material to EXAFS measurements. Powder neutron diffraction measurements on this $Fe_3(P_2O_7)_2$ polycrystal have been published elsewhere.[11] The average structural properties have already been described in Sec. I. The near-neighbor environment around the iron atoms is complicated, with two oxygen shells in the Fe^{2+} trigonal prism and six distinct Fe–O distances in the distorted Fe^{3+} octahedra. There are also several Fe–P distances. Since the intrinsic resolution of EXAFS measurements is not as good (in this case, ~0.1 Å) as the diffraction, we group the distinct shells into fewer "average" shells, with static radial-distribution widths. This procedure allows for direct comparison of the EXAFS and diffraction results. We refer to the three near-neighbor Fe–O shells as Fe–O_s, Fe–O_m, and Fe–O_l for short, medium, and long distances. These averaged diffraction measurements are presented in Table III.

Figure 7 shows the EXAFS data plotted as $k^3\chi(k)$ versus k from ferric ferrous pyrophosphate and the base glass as an example of the data quality. Figure 8 shows the Fourier transform (FT) of $k^3\chi(k)$ from $Fe_3(P_2O_7)_2$ and the fit, together with the individual contributions from each fitted scattering path. The peaks correspond to neighboring atoms around the central absorbing atom, phase shifted to lower r by the central and backscattering atomic potentials (usually between 0.1 and 0.4 Å). The FT differs from a true radial-distribution function because different species of backscattering atoms have different functional forms for the peak shape, and overlapping backscattering peaks may also cause interference patterns. Fits are therefore required to accurately interpret the data. The first peak from the crystal in Fig. 8 is primarily due to neighboring oxygen near 1.9 Å. The second peak (at ~2 Å in the FT) is a combination of a lobe from the Fe–O atomic distance of 1.9 Å and a broad oxygen peak corresponding to oxygen neighbors ~2.2 Å away from the absorbing iron. The peak at ~3 Å is primarily due to Fe at ~3 Å, but contains significant amplitude from phosphorus at 3.4 Å.

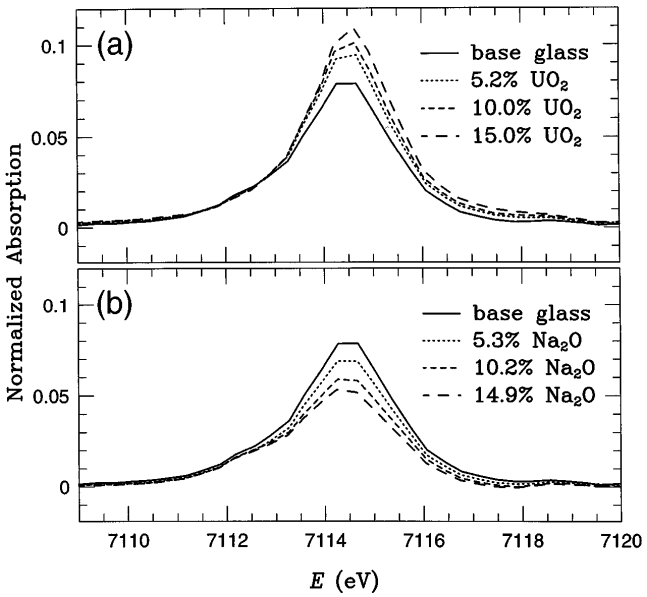

FIG. 6. Normalized absorption versus E with main edge removed for (a) the base glass with UO_2 and (b) the base glass Na_2O. Notice that the shoulder at 7112.4 eV decreases in amplitude as the main peak at 7114.5 eV increases and (from Fig. 3) the iron valence state increases.

TABLE III. $\langle N \rangle$ represents the number of such shells per iron atom. The Debye–Waller parameter (σ) reported for diffraction[11] is estimated only from the distribution of bond lengths within a specified shell, and does not include any contribution from the thermal parameters. EXAFS measurements of $\langle N \rangle$ assume an $S_0^2 = 0.75$, estimated from the reference compounds.

	$Fe_3(P_2O_7)_2$ polycrystal from diffraction			$Fe_3(P_2O_7)_2$ polycrystal from EXAFS			Iron-phosphate glass from EXAFS		
Path	$\langle N \rangle$	R (Å)	σ (Å)	$\langle N \rangle$	R (Å)	σ (Å)	$\langle N \rangle$	R (Å)	σ (Å)
Fe–O_s	2.66	1.908	0.057	3.0(3)	1.91(1)	0.073(5)	3.4(4)	1.90(1)	0.070(5)
Fe–O_m	2.00	2.197	0.028	2.0(6)	2.12(3)	0.07 (1)	0.8(2)	2.11(3)	0.08 (2)
Fe–O_l	1.33	2.404	0.020	0.8(3)	2.41(3)	0.07 (1)	0.6(2)	2.35(5)	0.07 (2)
Fe–Fe	1.00	3.115	0.0	1.0(3)	2.97(5)	0.09 (2)	0.2(1)	3.2 (1)	0.07 (3)
Fe–P	2.66	3.227	0.021	6 (2)	3.43(5)	0.09 (3)	3 (1)	3.18(4)	0.09 (2)
Fe–P	3.33	3.490	0.074				3 (1)	3.41(4)	0.09 (2)

Fit results from the $Fe_3(P_2O_7)_2$ data are displayed in Table III, together with results from our diffraction measurements. The diffraction[11] and EXAFS measurements concur about the local structure of $Fe_3(P_2O_7)_2$, including the long Fe–O distance at 2.4 Å, which was not found by the previous diffraction study.[9] This discrepancy could result from a difference in sample preparation techniques.

2. Base glass and comparison to $FePO_4$

The glass data (Fig. 9) are different from the data from $Fe_3(P_2O_7)_2$ in several respects. First, amplitude is shifted out of the second oxygen shell at ~2.2 Å and possibly into the first shell. Second, the average Fe–O near-neighbor distance is shorter in the glass (visible from the shift of the real part of the FT where it crosses zero at ~1.5 Å). Also, the Fe–P peak is diminished, but still visible, and finally, the Fe–Fe peak is greatly suppressed. The first and second points are mutually supporting evidence; if weight is shifted out of the second shell, the average position of the two shells will be shorter. Fits to the base glass reported in Table III reflect this description of the FT data.

The key to determining the dominant oxygen coordination in the base glass is to compare the glass data to data from $FePO_4$. Figure 9 shows that the near-neighbor oxygen environment is very similar in the two

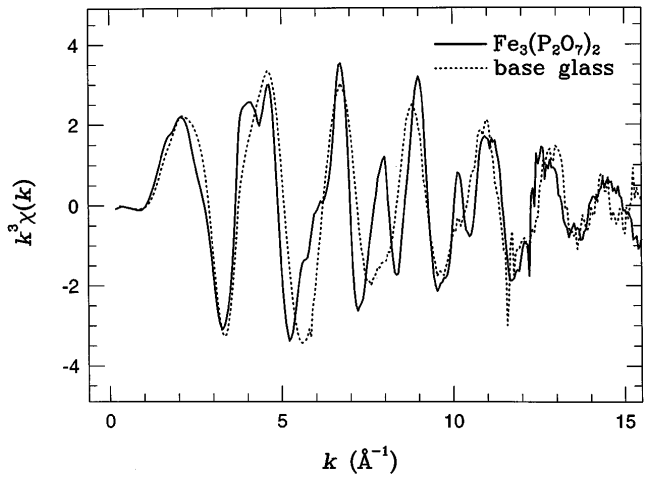

FIG. 7. $k^3\chi(k)$ versus k for the $Fe_3(P_2O_7)_2$ (solid) and the base glass (dotted). Notice the almost complete lack of a frequency in the glass as seen from the change in the peaks at ~4, 6, 8, and 10 $Å^{-1}$.

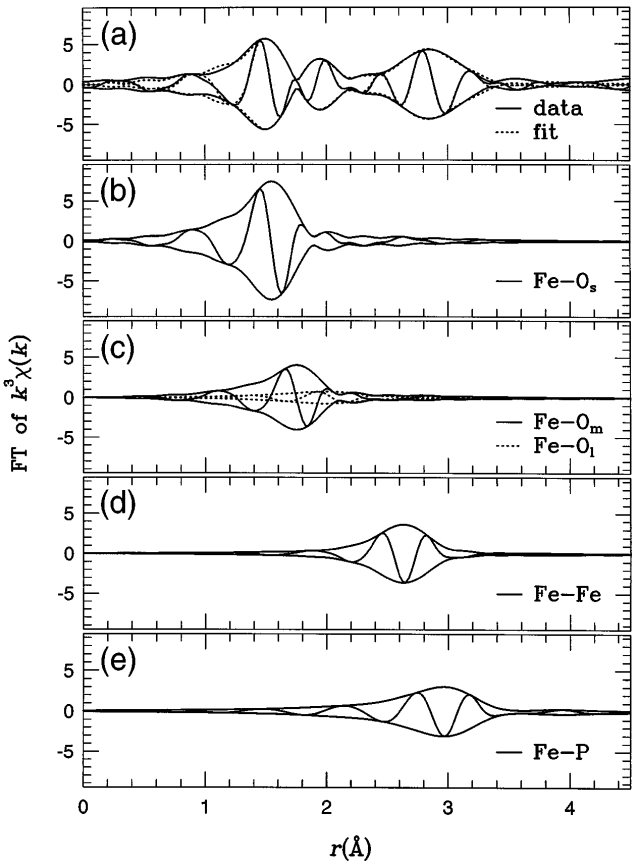

FIG. 8. Fourier transform (FT) of $k^3\chi(k)$ for the $Fe_3(P_2O_7)_2$ polycrystal, and the individual components from each scattering path. The outer envelope is the amplitude $[(Re^2 + Im^2)^{1/2}]$ of the transform, and the oscillatory part is the real part of the transform. The panels show (a) data (solid) and total fit (dotted), and (b)–(e) the individual peak fit functions, as indicated. Transforms are from 4.5–15 $Å^{-1}$ (Gaussian broadened by 0.3 $Å^{-1}$).

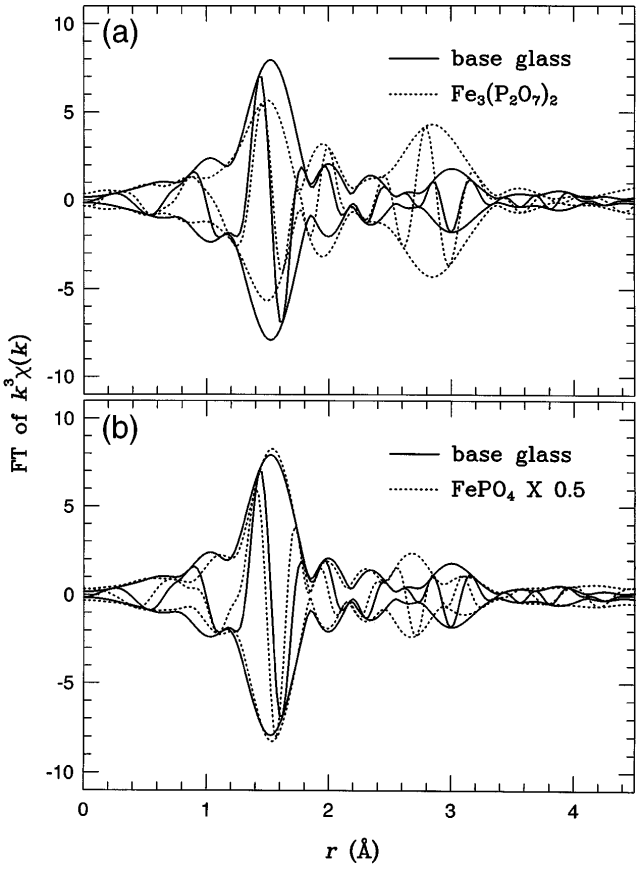

FIG. 9. FT of $k^3\chi(k)$ for the base glass (solid) and (a) the $Fe_3(P_2O_7)_2$ polycrystal (dotted) and (b) the $FePO_4$ polycrystal (dotted), which has been reduced by a factor of two. Differences in the real part between the glass and $FePO_4$ can be explained with a 4 eV shift of E_0 between the data sets.

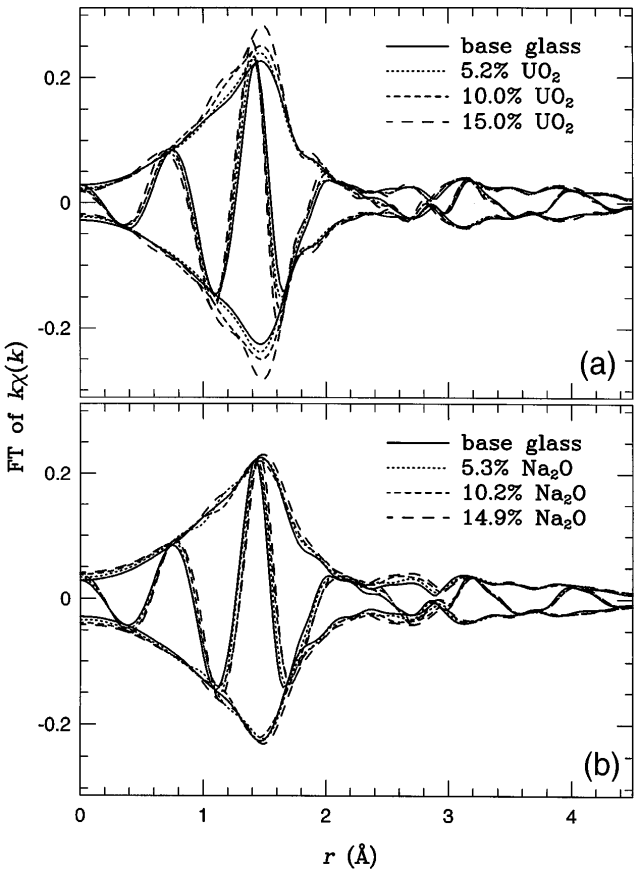

FIG. 10. FT of $k\chi(k)$ for the waste-form glass series. Notice that k-weighting is used (instead of k^3) to focus on the nearest-neighbor peaks. The figure shows (a) the base glass with UO_2 and (b) the base glass with Na_2O. The amplitude decreases and the phase (note the zero crossings of the real part) increases as series goes from $UO_2 \rightarrow Na_2O$.

samples. These data are very strong evidence that many of the iron sites in the base glass have tetrahedral oxygen coordination. The Fe–O environment can be fit with a combination of data from tetrahedral (from $FePO_4$) and octahedral (from $FePO_4 \cdot xH_2O$) reference materials. A reasonable fit is obtained with between 25 and 50% of the iron in tetrahedral sites, as discussed in Sec. IV. A.

3. Effect of adding UO_2 or Na_2O

Figure 10 shows the FT of $k\chi(k)$ of the glass series. We choose to use $k\chi(k)$ rather than $k^3\chi(k)$ to emphasize the Fe–O contribution to the spectrum. The amplitude of the first peak in the FT increases with increasing UO_2 and decreases with increasing Na_2O. A similar trend can be seen in the Fe–O_s bond length. Shifts in interatomic pair distances are easily observed by looking at the real part of the FT where it crosses zero amplitude. The first peak zero-crossing shrinks with increasing UO_2 and grows with Na_2O. Without performing any fits, these results can be interpreted in at least two ways: The nearest-neighbor Fe–O distance may shrink with increasing UO_2, or the Fe–O distribution may be distorted and weight is shifted from the further bonds to the shorter bonds in the radial pair-distribution.

Fits indicate no observable trends in the nearest-neighbor Fe–O number of neighbors $\langle N \rangle$, with $N = 3.6 \pm 0.9$ across the series, although the distribution of N has a rather large uncertainty. Given that the number of neighbors remains constant for this shell, we ascribe the change in amplitude to a combination of a narrowing distribution of Fe–O at ~1.9 Å, and the changing interference between the Fe–O_m and Fe–O_l scattering paths. We limit the correlation between N and σ by holding N fixed for subsequent fits. Figure 11 shows fit results for σ and $R_{\text{Fe–O}}$ as a function of UO_2 and Na_2O concentration. As Na_2O is added to the base glass, the average bond length contracts and the distribution widens. Just the opposite occurs when UO_2 is added to the base glass.

Fits to the Fe–O_m shell detect no change with substitution within the error limits in Table III. There are

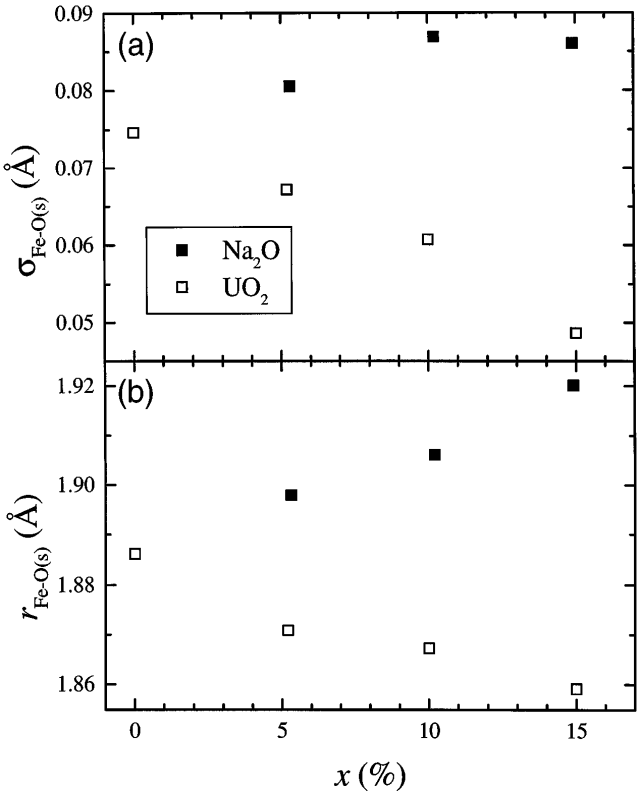

FIG. 11. Some fit results on the glass series: (a) $\sigma(\mathrm{Fe-O}_s)$ versus x, and (b) $R(\mathrm{Fe-O}_s)$ versus x.

visible changes in the EXAFS for the Fe–O_l, Fe–P, and Fe–Fe region (Fig. 10); however, correlations between the fit parameters for these peaks (and to a lesser degree, the Fe–O_l peak) make quantifying these changes extremely difficult for this data set.

IV. DISCUSSION

The primary goal of this study is to characterize the local structure around the iron atoms in the iron-phosphate glass samples. This information adds to the structural basis for understanding the enhanced chemical durability of these glasses. There are several structural questions that can be addressed: How do the Fe^{2+} ions affect the average structure, and what is the oxygen coordination of these sites? As the number of Fe^{2+} ions changes, is the distribution around Fe^{3+} ions affected? How does the local structure of the glasses compare with crystalline counterparts? Lastly, what does the further neighbor environment look like, especially the Fe–P distribution? These central issues will be discussed in terms of the XANES and EXAFS results.

A. Iron coordination and individual iron sites

As the valence varies from sample to sample, so do both XANES and EXAFS features in the absorption spectrum. To interpret the pre-edge features correctly, we first must determine which site(s) are responsible for the specific features. We can unambiguously assign the main peak in the pre-edge of all the glass samples to Fe^{3+} because its position matches that of the Fe^{3+} reference samples, and because its amplitude increases with valence (increasing UO_2). In addition, the smaller peak present in the samples with Fe^{2+} decreases with increasing Fe^{3+}.

The low-energy pre-edge feature is consistent with the Fe^{2+} atoms in an octahedral coordination. This interpretation is supported by the amplitude and energy position of the smaller (first) peak in the 15% Na_2O glass. The amplitude of this peak per Fe^{2+} is $0.012/0.295 = 0.041(3)$, which is consistent with the amplitude of the left lobe in FeO and Fe^{2+} in 1.5 M $HClO_4$, as is the energy of the excitation.

We can apply this knowledge of the pre-edge features and combine it with the local structure data to make a strong argument for a large number of iron atoms in the trivalent state with tetrahedral oxygen coordination. We know both from the Fe K-edge energy and the Mössbauer results that the iron atoms in the base glass are mostly Fe^{3+}. We have shown that the nearest-neighbor oxygen environment is very similar to that in $FePO_4$; that is, many of the iron atoms are in a tetrahedral coordination in agreement with the analysis of the pre-edge features in Sec. III. A. 2. Moreover, the EXAFS results are in quantitative agreement, both by comparison to $FePO_4$, and from fits which give the total number of Fe–O neighbors in the glass to be 4.8 ± 0.5. We therefore estimate that 25–50% of the irons are Fe^{3+} ions sitting on tetrahedral sites. That leaves 25–50% irons as Fe^{3+} in possibly distorted octahedral sites and 25% as Fe^{2+} in roughly undistorted octahedral sites. The ranges are broad because it is impossible to know what type of distortion of the octahedra occurs around Fe^{3+} ions. However, the XANES data indicate the distortion is much less than in, for instance, Fe_2O_3.

Changes in the local oxygen environment when Na_2O or UO_2 are added to the glass are at least partially due to changes in the mean iron valence. As the valence becomes closer to trivalent, the Fe–O peak amplitude in the EXAFS (Fig. 10) becomes larger. This increase in amplitude could either be due to an increase in the number of tetrahedral sites (taking weight out of further peaks and putting weight into the closest peak) or due to removing some of the possible distortions of octahedral sites [consider Fig. 11(a)]. However, if the octahedral distortions are partially removed, the mean bond length probably should increase, contrary to measurement [Fig. 11(b)]. The simplest, most consistent explanation is that as Fe^{2+} sites are converted to Fe^{3+} sites, many of these sites have tetrahedral coordination, thereby increasing the relative fraction of tetrahedral-coordinated iron sites.

Since $Fe_3(P_2O_7)_2$ has the only example of Fe^{2+} in a trigonal prism arrangement, the contribution to the pre-edge feature for this site should be considered. The Fe^{2+} feature (the first peak) in the XANES data for this sample is associated with this coordination. Other contributions may be included in the second peak. The trigonal prism contribution to the first peak appears to be similar to an octahedral contribution in energy, but the peak amplitude of 0.05(1), again corrected for Fe^{2+} concentration, may be higher.

B. Further neighbor environment from EXAFS

The lack of an appreciable number of iron neighbors and the presence of phosphorus neighbors (Table III) indicates that each of the Fe–O–P linkages in the glass usually contains only a single iron atom. This distribution may indicate a $FeO_6–P_2O_7–FeO_6–P_2O_7$ network is formed in the glasses [as in $Fe_3(P_2O_7)_2$] with short-range order, but they no longer occupy three adjacent layers, that is, chains of $\ldots–FeO_6–FeO_6–\ldots$ no longer form. The presence of a similar number of Fe–O–P links in the glass as in the crystal is consistent with models that require many such links for good chemical durability.

The data from the pyrophosphate polycrystal provide interesting clues regarding the local structure of iron in the glasses. From the discussion above, ferric ferrous pyrophosphate has a very similar Fe–P environment to the base glass, yet the Fe–O and Fe–Fe environments are clearly different (Fig. 9). The central issue behind understanding how the structure and the chemical durability of these glasses are related is determining whether PO_4^{3-} can link together to form large channels, or if enough NBOs form to prevent such channels. From a local structure point of view, a necessary consequence of NBOs is several Fe–O–P linkages per Fe. We have shown that for these glasses, most of these Fe–O–P linkages are preserved in the glass compared to the prototypical crystal $Fe_3(P_2O_7)_2$. These links exist with up to 15% Na_2O or UO_2. With so many Fe–O–P links, the irons must act as cross-links between PO_4^{3-}, and may also help terminate PO_4^{3-} chains.

Although there are several Mössbauer, ir, and other studies of the local structure around iron in the literature, there are few with which to compare to this study because of the wide variability in sample preparation. The iron-phosphate glasses used in Ref. 8 include one with a similar starting composition to our base glass, and was prepared under similar conditions. The Mössbauer spectra indicate a tetrahedral Fe^{3+} coordination, in addition to Fe^{2+} and Fe^{3+} octahedral coordinated atoms. The results of this previous study are therefore in qualitative agreement with those presented here, although there are differences in the interpretation of the Mössbauer data.

V. CONCLUSION

We have determined the local near-neighbor distribution around iron for iron-phosphate glasses with various amounts of UO_2 and Na_2O, and compared these distributions to a ferric ferrous pyrophosphate polycrystal and other iron oxides. Both EXAFS and XANES are consistent with a 6-fold oxygen-coordinated Fe^{2+} site and Fe^{3+} sites roughly split between those with tetrahedral and those with octahedral coordination. Fe–P atom pairs were observed in all samples, indicative of Fe–O–P linkages. These Fe–O–P links appear not to be affected by loading. The main effect of loading with UO_2 or Na_2O was found to be a mean valence shift toward (for UO_2) or away (for Na_2O) from Fe^{3+} in a way that roughly maintains the relative number of tetrahedral and octahedral Fe^{3+} sites. These sorts of changes preserve the important Fe–O–P linkages which contribute to the enhanced chemical durability of these glasses, even under loading. These results are a step toward a firm understanding of the exceptional durability of iron-phosphate glasses, even under loading.

ACKNOWLEDGMENTS

This work was supported by the Director, Office of Energy Research, Office of Basic Energy Sciences, Chemical Sciences Division of the United States Department of Energy under Contract No. DE-AC03-76SF00098. X-ray-absorption measurements were done at SSRL, which is operated by the Department of Energy, Office of Basic Energy Sciences under Contract No. DE-AC03-76SF00515.

REFERENCES

1. B. C. Sales and L. A. Boatner, Science **22**, 45 (1984).
2. B. C. Sales and L. A. Boatner, J. Non-Cryst. Solids **71**, 103 (1985).
3. B. C. Sales and L. A. Boatner, J. Non-Cryst. Solids **79**, 83 (1986).
4. B. C. Sales, R. S. Ramsey, J. B. Bates, and L. A. Boatner, J. Non-Cryst. Solids **87**, 137 (1986).
5. "Storage & Disposition Final Programmatic Environmental Impact Statement," Department of Energy EIS 0229–Implementation Plan (S&E PEIS, DOE/EIS-0229), Dec. 1996.
6. G. N. Greaves, S. J. Gurman, L. F. Gladden, C. A. Spence, P. Cox, B. C. Sales, L. A. Boatner, and R. N. Jenkins, Philos. Mag. B **58**, 271 (1988).
7. A. Osaka, K. Takahashi, and M. Ikeda, J. Mater. Sci. Lett. **3**, 36 (1984).
8. W. Guomei, W. Yuan, and J. Baohui, *Proceedings of the SPIE* **2287**, 214 (1994).
9. M. Ijjaali, G. Venturini, R. Gerardin, B. Malaman, and C. Gleitzer, Eur. J. Solid State Inorg. Chem. **28**, 983 (1991).
10. G. Concas, F. Congiu, E. Manca, C. Muntoni, and G. Pinna, J. Non-Cryst. Solids **192 & 193**, 175 (1995).
11. G. K. Marasinghe, M. Karabulut, C. S. Ray, D. E. Day, M. G. Shumsky, W. B. Yelon, C. H. Booth, P. G. Allen, and D. K. Shuh, J. Non-Cryst. Solids **222**, 144 (1997).
12. A. Musinu, G. Piccaluga, and G. Pinna, J. Non-Cryst. Solids **122**, 52 (1990).
13. F. d'Yvoire, Bull. Soc. Chim. Fr. **1862**, 1224 (1962).

14. Sample as obtained from Alfa Aesar is a powder with unknown H_2O content. EXAFS determines a local structure that does not agree with diffraction literature. We use the sample here as a good example of Fe^{3+} in octahedral coordination, as shown by the EXAFS, and are not concerned with the long-range structure.
15. H. N. Ng and C. Calvo, Can. J. Chem. **53**, 2064 (1975).
16. T. M. Hayes and J. B. Boyce, in *Solid State Physics*, edited by H. Ehrenreich, F. Seitz, and D. Turnbull (Academic, New York, 1982), Vol. 37, p. 173.
17. G. G. Li, F. Bridges, and C. H. Booth, Phys. Rev. B **52**, 6332 (1995).
18. J. Wong, F. W. Lytle, R. P. Messmer, and D. H. Maylotte, Phys. Rev. B **30**, 5596 (1984).
19. A. Mancau, A. I. Gorshkov, and V. A. Drits, Am. Miner. **77**, 1133 (1992).
20. T. E. Westre, P. Kennepohl, J. G. DeWit, B. Hedman, K. O. Hodgson, and E. I. Solomon, J. Am. Chem. Soc. **119**, 6297 (1997).
21. J. J. Rehr, private communication.
22. R. G. Shulman, Y. Yafet, P. Eisenberger, and W. E. Blumberg, Proc. Natl. Acad. Sci. U.S.A. **73**, 1384 (1976).
23. K. Rahkonen and K. Krause, Atomic Data and Nuclear Tables **14**, 139 (1974).
24. S. I. Zabinsky, A. Ankudinov, J. J. Rehr, and R. C. Albers, Phys. Rev. B **52**, 2995 (1995).
25. Differences in E_0 in Ref. 11 are because Fe_2O_3 was used as the Fe^{3+} reference compound.
26. I. D. Brown and D. Altermatt, Acta Crystallogr. B **41**, 244 (1985).